CHEMISTRY OF MATERIALS

pubs.acs.org/cm

Article

Temperature-Dependent Capsule Shell Bonding and Destruction Based on Hindered Poly(urea-urethane) Chemistry

Yifei Wang, Peiran Wei, Qing Zhou, Ciera Cipriani, Miao Qi, Svetlana Sukhishvili, and Emily Pentzer*

Cite This: *Chem. Mater.* 2022, 34, 5821−5831

Read Online

ACCESS | Metrics & More | Article Recommendations | Supporting Information

ABSTRACT: Capsules with responsive shells that, for example, can be destroyed to release a payload or fused together to create a monolith are needed to improve performance in, for example, controlled release, material storage/transport, molecular separation, and so on. Most commonly, these shells contain pH-responsive functional groups or temperature-responsive polymers and undergo changes in shell permeability, for example, upon decreased pH or increased temperature. Herein, we report a new approach to fabricating responsive capsules for controlled fusion or destruction by the incorporation of hindered poly(urea-urethane) chemistry into capsule shells. Using a non-aqueous Pickering emulsion as a template, we demonstrate that interfacial polymerization between three different secondary diamines and four different diisocyanates can be used to prepare capsules with a core of polar oil (*N*,*N*-dimethylformamide, DMF) or a mixture of DMF and ionic liquid (IL) with shells containing hindered urea bonds that undergo dynamic bond exchange in response to slightly elevated temperatures. For the capsules in which the core is oil, the temperature of responsivity is based on the hindrance of the diamine (35, 55, or 80 °C), consistent with the bulk polymer, and supported by variable-temperature Fourier transform infrared spectroscopy. In contrast, for capsules in which the core contains IL, the temperature required is significantly decreased, suggesting that the shell is plasticized with the core liquid. Heating isolated capsules to the relevant temperature leads to capsule shell fusion into a monolith, whereas addition of a primary amine to dispersed capsules at elevated temperature leads to shell destruction. Scanning electron microscopy (SEM) and optical microscopy were used to confirm the morphology of capsules, monoliths, or emulsion droplets, and focused ion beam-SEM was utilized to demonstrate the core-shell structure of the capsules. Furthermore, comparison of mechanical tests of the capsules and fused monoliths highlight the importance of bond exchange on bulk properties. This work demonstrates that capsule shells containing dynamic covalent bonds are a new exciting class of materials that can be used to tailor morphology beyond the traditional use of responsive shells to change permeability.

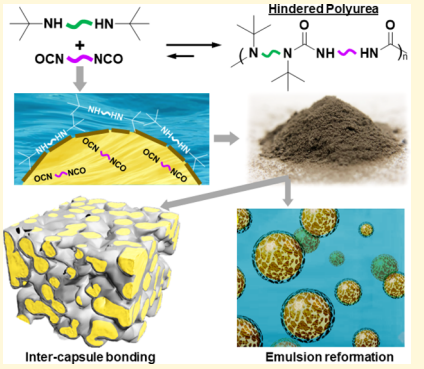

INTRODUCTION

Capsules with responsive shells have earned increasing attention in the past decades because of their promising applications in targeted delivery,[1,2] controlled release,[3−6] energy transport/storage,[7] etc. To impart capsule shells with chemical bond dynamicity, researchers have established various methodologies, including incorporating stimuli-responsive small molecules or anchoring reactive molecules and initiators onto the shell.[8−11] For instance, Kitayama and Harada prepared capsules via interfacial photo-crosslinking of 2-diethylaminoethyl methacrylate and 2-cinnamoylethyl methacrylate, where protonation and deprotonation of the tertiary amine group controlled the shrinking and swelling of the capsules and thus cargo release.[9] Additionally, polymer capsules with surface morphology responsive to temperature were successfully constructed by Zeng et al. by depositing polydopamine functionalized with 2-bromoisobutyryl bromide onto SiO_2 particles, followed by surface-initiated growth of poly-*N*-isopropylacrylamide.[10] Yao et al. prepared "gated" capsule shells with reversible pore formation controlled by a photo-sensitive azobenzene-containing surfactant, which could eliminate excessive reactive oxygen in cellular biomolecules upon the release of encapsulated cysteamine.[11] Most studies in the area of responsive capsule shells focus on employing reactive small molecules, functional groups, and stimuli-responsive polymers for configuration change. Motivated to expand capsule versatility and to equip capsule shells with multiple transformation pathways (e.g., shell bonding in a solid state, morphology change with easy-to-apply stimuli), we sought to prepare capsules with polymeric shells containing dynamic covalent bonds and demonstrate both inter-capsule crosslinking into monoliths and destruction of capsule shells.

Generally, capsules are synthesized by one of three ways: (1) the hard-template method[12−14] or shell formation on a

Received: February 8, 2022
Revised: June 18, 2022
Published: June 28, 2022

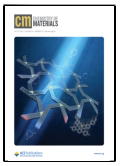

Scheme 1. (A) Illustration of Irreversibility and Reversibility of Non-Hindered and Hindered Polyurea Chemistries, Respectively; (B) Schematic of Capsule Preparation, Isolation, and the Use of the Dynamicity of the HUBs in the Capsule Shell to Produce Monoliths or Destroy Capsule Shells

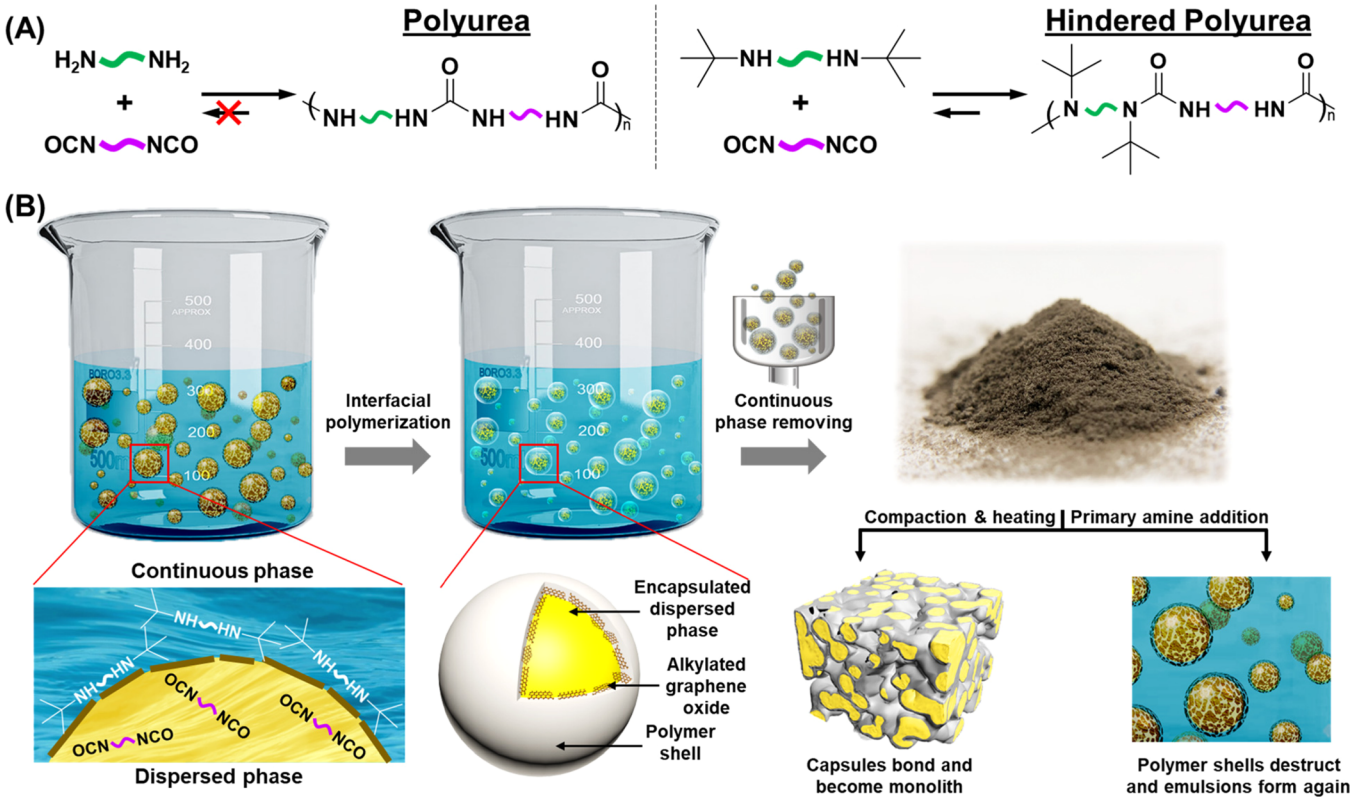

sacrificial core and then core removal, (2) the soft-template method[15−17] or interfacial polymerization within an emulsion, or (3) the microfluidic method[18] where liquid monomers are crosslinked at an emulsion droplet interface produced in flow. Among these, the soft-templated method has garnered significant attention due to a relatively simple experimental procedure and lack of need for complicated infrastructure or template removal. For example, Yi et al. fabricated microcapsules through interfacial and in situ polymerization of a melamine formaldehyde prepolymer in an oil-in-water emulsion stabilized by lignin nanoparticles.[19] The capsules were loaded with isophorone diisocyanate and then incorporated into an epoxy resin, with the capsules holding a "healing agent" for damage. In a similar vein, Weiss et al. successfully produced capsules with cores of ionic liquid (IL) using IL-in-water emulsions stabilized by lignosulfonic acid; in this case, polycondensation of tetraethoxysilane at the fluid−fluid interface gave a silica shell and the capsules were used for the heterogenization of a palladium catalyst for hydrogenation of alkynes.[20] Furthermore, Landfester and colleagues prepared glycerol-encapsulated nanocapsules through interfacial polyaddition of glycerol and toluene diisocyanate using an oil-in-water emulsion stabilized by polyglycerol polyricinoleate, where the capsules can be used for improving the lubricant performance in metal−metal contact cases.[21] Additionally, the Pentzer group constructed capsules from Pickering emulsions stabilized by 2D particles using interfacial polymerization between diisocyanate and diamine in oil/water,[22] oil/oil,[23] IL/water,[15] and IL/oil[15] systems, with the identity of the two phases dependent on the nanosheet functionalization. Using these systems, Luo et al. and Edgehouse et al. produced capsules with composite shells of polyurea and nanosheets and cores of IL or polyalpholefin for use in CO_2 uptake[24,25] and benzene removal from water,[22] respectively. The ability to tailor not only the composition of the shell and core of the capsules but also their responsiveness to external stimuli will have broad impact across many fields.

Dynamic covalent bonds (DCBs) undergo efficient bond exchange through an associative or dissociative mechanism in response to an external stimulus.[26,27] The most prevalent DCB mechanisms are based on boronic esters,[28,29] disulfides,[30,31] imines,[32] Diels-Alder (D-A) adducts,[33,34] and olefin metathesis[35] reactions. When incorporated into polymers, DCBs can be used to tune stimuli-responsive properties and produce materials for specific applications.[36] For example, Accardo and Kalow successfully achieved a photocontrolled hydrogel which underwent softness-stiffness variation based on boronic ester crosslinking.[37] Alternatively, Konkolewicz et al. fabricated dynamic interpenetrated networks by combining thermoresponsive D-A reactions and hydrogen bonds, where the materials showed great self-healing capabilities and the mechanical properties were adjusted by changing the crosslinker content and chain length.[38] Similarly, the Sukhishvili lab employed D-A chemistry to prepare a 3D printable self-healing and reprogrammable material.[39] One intriguing type of DCB is the hindered urea bond (HUB)[40−42] or ureas formed by the reaction of a secondary amine and isocyanate. In contrast to ureas produced by the reaction of a primary amine and isocyanate, HUBs are thermally reversible (Scheme 1A). Such dynamicity is attributed to the disruption of the planarity of the urea bond due to the presence of a relatively bulky group attached to the nitrogen atom.[43,44] The specific mechanism of

https://doi.org/10.1021/acs.chemmater.2c00415
Chem. Mater. 2022, 34, 5821−5831

reversion of the HUB to the secondary amine and isocyanate is still not clear and may be associative or dissociative based on reaction conditions (solvating environment, presence of a catalyst, identity of amine and isocyanate, etc.).[45−47] To date, HUBs have been incorporated into bulk polymers and used for self-healing, shape memory, and in coating materials. For example, Ying et al. prepared a hindered poly(urea-urethane) which can recover up to 87% of its original mechanical strength after cutting and healing at 37 °C for 12 h.[44] Likewise, Sun and co-authors incorporated HUBs into PDMS; with the addition of a graphene filler, a healable and recyclable conductive composite was produced.[48] To date, the focus of DCBs in polymers has been in bulk systems.

This research presented herein focuses on the application of dynamic covalent chemistry in polymer capsule shells, rather than bulk polymers, providing a new class of responsive material constructs. We report the production of capsules containing composite shells of hindered poly(urea-urethane)s (HPUU) templated by water-free Pickering emulsions stabilized by graphene oxide (GO)-based nanosheets and examine the temperature-responsive features of capsules with different shell composition and core materials. This builds upon our recent communication that capsule shells prepared with isopropyl ethylenediamine and diisocyanate can have dynamic exchange ability.[23] Capsules with a liquid core and DCB-containing shell undergo bond exchange to give monoliths, or destruction to produce simple emulsions (Scheme 1B). The use of non-aqueous emulsions ensures that diisocyanate monomers can be used without hydrolysis by water. Dynamic capsules with different temperatures of response were obtained by controlling both the steric demands of the amines and the identity of the liquid core. Capsule shell fusion provides a new route to transform a powder into a monolith, which can enable handling of the liquid as a solid and is relevant for integration of liquids into applications that require dry feedstock.[49] Additionally, these dynamic capsules could also find use as feedstocks for producing composites by additive manufacturing (e.g., direct ink writing[50,51]), without the use of high temperature, high pressure, or UV irradiation. Alternatively, shell destruction can be used to release capsule contents. This new approach to responsive polymer capsule shells has applications across energy storage/transport, controlled release, and additive manufacturing and should be applicable to other emulsion systems, 2D particles, and reagents.

EXPERIMENTAL SECTION

Materials. *N*,*N*-Di-*tert*-butyl ethylenediamine (DTEDA, >98.0%) was from TCI Chemical. *N*,*N*-Di-isopropyl ethylenediamine (DIEDA, 99.0%), hexamethylene diisocyanate (HDI, ≥99.0%), dibutyltin diacetate (DBTDA), graphite flakes, sulfuric acid (H_2SO_4), potassium permanganate ($KMnO_4$, ≥99%), propylamine (98.0%), and hexane (≥98.5%) were all purchased from Sigma Aldrich. *N*,*N*-Di-ethyl ethylenediamine (DEEDA, 95.0%), 1,3-bis(isocyanatomethyl)-cyclohexane (CHDI, ≥99.0%), *m*-xylylene diisocyanate (mXDI, ≥98%), *N*,*N*-dimethylformamide (DMF, anhydrous, ≥99.8%), tetra-(ethylene glycol) (TEG, 99.0%), triethanolamine (TEA, ≥98.0%), hydrogen peroxide (H_2O_2, 30% w/w), hexylamine (99%), dodecane (≥99.0%), isopropanol (≥99.5%), toluene (≥99.5%), and DMF (≥99.8%) were all bought from Fisher Scientific. 1,3-Bis(2-isocyanato-2-propyl)benzene (BZDI, ≥97.0%) was purchased from VWR. Octadecylamine (95.0%) and octane (99.0%) were from Oakwood Chemical. 1-Hexyl-3-methylimidazolium bis-(trifluoromethylsulfonyl)imide ([Hmim][TFSI], 99.0%) was purchased from Iolitec. All reagents were used as received, without further purification.

Instrumentation. Reagent homogenization for bulky polymer synthesis was achieved by a Conditioning Mixer purchased from Thinky Corporation (model AR-100). Sonication was done through an ultrasonic bath (model CPX 3800) and vortexing was accomplished by a vortex (model 9454FIALUS), where both were from Fisherbrand. Centrifugation was performed by a centrifuge from Thermo Scientific, model 75005703. Blending of GO flakes was done using a Waring Commercial blender (model 7010S). Emulsification was completed by a hand-held tissue-tearor from Biospec Product Inc. (model 985370). Optical microscopy images were taken using a microscope from Amscope attached with an A35180U3 camera from Amazon. Fourier transform infrared (FTIR) spectroscopy was performed using a JASCO FTIR spectrometer, model FTIR-4600LE MidIR. Variable-temperature FTIR (VT-FTIR) spectroscopy was performed using the JASCO FTIR equipped with a varied-temperature setup (Figure S1), where power source (brand SmoTecQ, model 4336304932), variable resistor (manufacturer Elenco Electronics Inc., model RS500), test lead set (manufacturer Elenco-THI, model TL-16), heating plate (brand Zerodis, model Zerodis7i2r1quwgt-02), and IR resolution thermal camera (manufacturer Xintest, model HT-A2) were all from Amazon. Compression test was achieved using a DMA 850 instrument, and TGA was carried out using a TGA 5500 instrument from TA Instruments in the Soft Matter Facility at Texas A&M University. ^{1}H NMR for IL percentage measurement was done using Avance NEO 400 instruments. Sputter coating was done by a Cressington 108 Sputter Coater, and scanning electron microscopy (SEM) characterization was performed using a Tescan Vega3 instrument in the Microscopy and Imaging Center at Texas A&M University. Focused ion beam (FIB)-SEM was done using a Tescan LYRA-3 Model GMH Focused Ion Beam Microscope in the Materials Characterization Facility and a FEI Helios Nanolab 460F1 Dual-Focused Ion Beam Microscope in the AggieFab Nanofabrication Facility at Texas A&M University.

Synthesis of Graphene Oxide. The preparation of GO was achieved through a previously published modified Hummer's method.[52] Concisely, graphite flakes (1.0 g) were first mixed with H_2SO_4 (133.0 mL), followed by very slow addition of $KMnO_4$ (1.0 g). The addition of $KMnO_4$ (1.0 g) was repeated 3 times at 24 h intervals, and the reaction was kept at 25 °C during the whole synthesis process, after which a purple product was obtained. The reaction was quenched by slowly pouring the purple mixture into ice water (1.0 L), accompanied by continuous stirring, followed by dropwise addition of H_2O_2 until the color of the mixture turned light brown. The brown product was washed with isopropanol until litmus paper showed the pH reached nearly neutral. The final product was dried under reduced pressure at room temperature, and the dried flakes of GO were blended into powder which was stored at 2−8 °C.

Synthesis of Octadecylamine-Functionalized Graphene Oxide (C_{18}−GO). C_{18}−GO was synthesized through a method previously reported by the Pentzer lab. Initially, GO powder (96.0 mg) was dispersed in DMF (40.0 mL) by sonication, and octadecylamine flakes (0.9 g) were dissolved in DMF (60.0 mL) by stirring at 60 °C. Then, GO dispersion and octadecylamine solution were mixed and stirred at 55 °C for 30 min, followed by centrifugation to remove DMF and get dark brown precipitate. The precipitate was redispersed in toluene (50.0 mL) and mixed with another batch of octadecylamine (3.0 g dissolved in 50.0 mL of toluene). The mixture was stirred overnight at 55 °C, after which the dark brown precipitate was washed with toluene (100.0 mL) and octane (50.0 mL) twice. The final product was dispersed in 48.0 mL of octane to prepare a 2.0 mg/mL (standard by parent GO) C_{18}−GO/octane dispersion.

Preparation of Capsules from DMF-in-Octane and DMF/IL-in-Octane Emulsion Templates. Taking the DTEDA × HDI capsule as an example, synthesis steps were as follows. Anhydrous DMF (dispersed phase, 0.4 mL) was charged in a vial with the addition of HDI (115 μL, 0.718 mmol), TEG (68 μL, 0.393 mmol), and TEA (7.6 μL, 0.057 mmol). Reagents were homogenized under

https://doi.org/10.1021/acs.chemmater.2c00415
Chem. Mater. 2022, 34, 5821−5831

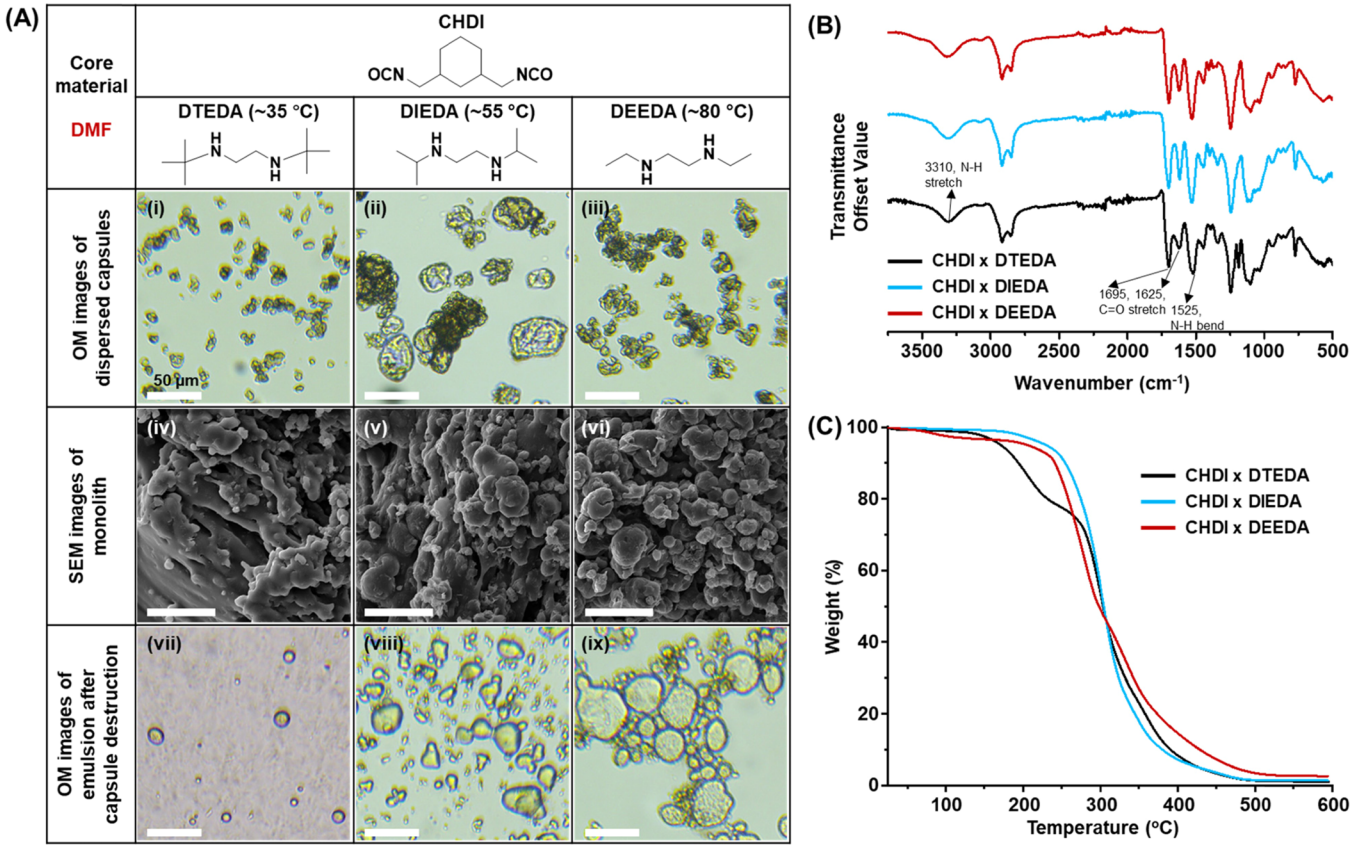

Figure 1. CHDI × DTEDA/DIEDA/DEEDA capsules with the DMF core: (A) Optical microscopy images of individual capsules redispersed in dodecane (i–iii), SEM images of monoliths (iv–vi), and optical microscopy images after shell destruction (vii–ix), scale bars are 50 μm; (B) FTIR spectra; and (C) TGA curves.

vortex for 30 s. 2.0 mL of C_{18}–GO/octane dispersion (2.0 mg/mL) was then added to the vial, followed by emulsification using a hand-held tissue-tearor for 25 s at maximum power to get a DMF-in-octane emulsion. Next, DTEDA (0.231 mmol, 50 μL) was dissolved in octane (0.5 mL), and the solution was added dropwise into the continuous phase (octane) of the obtained emulsion while swirling by hand. Finally, 0.7 μL of DBTDA was added. The emulsion was stored at 2–8 °C for 72 h for the completion of interfacial polymerization, after which the mixture was flushed with hexane. The reaction was then quenched by propylamine at 2–8 °C, and hexane was employed to remove extra propylamine. Finally, dry capsule powder was obtained under reduced pressure at ~5 °C. Capsules were stored at 2–8 °C to prevent undesired bond exchange. All other capsules were synthesized through the same procedure with adjusted diamine and diisocyanate amounts which can be found in Table S1. DMF/IL-in-octane-templated capsules were also achieved from the same method, where 0.1 mL of [Hmim][TFSI] was dissolved in 0.3 mL of DMF.

Capsule Shell Fusion and Destruction. Capsule shell fusion was performed by charging ~30 mg of capsules in a vial, where capsules were compacted through solvent (hexane) evaporation. Compacted capsules were heated (35 °C for DTEDA × HDI/CHDI/BZDI/mXDI capsules, 55 °C for DIEDA × HDI/CHDI/BZDI/mXDI capsules, and 80 °C for DEEDA × HDI/CHDI/BZDI/mXDI capsules) on a hot plate using a heating block for 24 h, after which dark monolithic samples can be observed. Capsule shell destruction was achieved by adding 400 μL of hexylamine to 30 mg capsules which were dispersed in 2 mL of octane and heating for 24 h at corresponding temperatures mentioned above.

Synthesis of Bulk Polymers. Bulky polymers were synthesized through a modified method previously reported from the Cheng group.[46] Taking the DTEDA × HDI bulky polymer as an example, the specific procedure was as follows. First, anhydrous DMF (0.17 mL, 2.1 mmol) was mixed with HDI (0.66 mL, 4.1 mmol) in a vial under stirring in an ice bath. Next, DTEDA (0.29 mL, 1.3 mmol) was added dropwise into the HDI/DMF mixture with the temperature strictly controlled at 0 °C. After adding the amine, the mixture was kept at 0 °C and stirred for 20 min. TEA (0.045 mL, 0.34 mmol), TEG (0.39 mL, 2.3 mmol), and DBTDA (0.0037 mL, 0.014 mmol) were then added to the above mixture, and all the reagents were homogenized using the Thinky Mixer at 400 rpm for 2 min. The final mixture was cured at room temperature under nitrogen gas protection overnight and then at 60 °C for another 12 h. Finally, a light yellow, transparent solid was obtained.

The synthesis of the DEEDA × HDI bulky polymer was performed following the same procedure with the amount of DEEDA as 0.18 mL and curing at 80 °C.

Compression Test for the Monolithic Sample and Capsule Powder. 30 mg DTEDA × mXDI capsule powder was put into a KBr pellet mold, through which a cylinder sample was obtained, as shown in Figure 6C (left). The cylinder sample was carefully moved to the DMA testing stage to avoid sample collapse. For the monolithic sample, 30 mg DTEDA × mXDI capsule powder was also put into the KBr pellet mold but followed by heating in a vacuum oven at 35 °C overnight, after which a dark monolithic sample was obtained (Figure 6B left). Samples were compressed from 0 to 45% strain at a rate of 45% per min.

VT-FTIR Spectroscopy. VT-FTIR measurement was achieved through a setup as shown in Figure S1. A power supply, variable resistor, heating film, and test lead set were connected to compose a variable-temperature device which was attached to the JASCO FTIR instrument. The temperature was controlled by adjusting the variable resistor and was real-time detected by an IR resolution thermal camera. When the desired temperature was achieved, samples were held at the temperature for 5 min before measurement was carried out.

https://doi.org/10.1021/acs.chemmater.2c00415
Chem. Mater. 2022, 34, 5821–5831

Table 1. Size Range for Different Capsule Samples as a Function of Diamine and Diisocyanate[a]

amine \ isocyanate	CHDI	HDI	BZDI	mXDI
DTEDA (~35 °C)	5 ~ 10 (μm)	5 ~ 25 (μm)	≤ 10 (μm) (20 ~ 25)	15 ~ 35 (μm)
DIEDA (~55 °C)	25 ~ 50 (μm)	25 ~ 50 (μm)	10 ~ 50 (μm) (15 ~ 20)	20 ~ 50 (μm)
DEEDA (~80 °C)	5 ~ 20 (μm)	20 ~ 40 (μm)	10 ~ 20 (μm) (25 ~ 40)	15 ~ 35 (μm)

[a]The size ranges in parentheses for BZDI column are for capsules with a core of DMF/IL.

Determining wt% IL Using ^{1}H NMR Spectroscopy. Measurement of IL% was achieved by extracting the [Hmim][TFSI] out of capsules using acetone-d^6 and calculated using mesitylene as an inner-standard content. Briefly, 42.9 mg mesitylene was dissolved in 7.0 mL of acetone-d^6, followed by ~20.0 mg capsules which were dispersed in 1.0 mL of mesitylene/acetone-d^6 solution. The mixture was then vortexed for 10 s and sonicated for 10 s alternately 3 times. A PTFE syringe filter (25 mm in diameter, 0.22 μm pore size) was then used to remove capsule shells, and a clear solution was obtained. From the ^{1}H NMR spectrum, the peak integral ratio of the *N*-methyl of [Hmim][TFSI] (3.65 ppm) to the methyl of mesitylene (2.09 ppm) was obtained for the calculation of IL% (Figure S2).

SEM Sample Preparation. A 7 mm × 7 mm conductive carbon double-sided tape attached stub (Ø12.7 mm × 8 mm pin height) was used as a sample substrate. For monolith, the 5 × 5 mm sample was put onto the conductive carbon double side tape with Au (20 nm thickness) sputter coating; to prepare the powder sample for FIB-SEM, particles were put onto the tape, and excess powder was blown away with nitrogen/air gas without any coating.

RESULTS AND DISCUSSION

Production of capsules from emulsion templates requires the use of a surfactant which suitably stabilizes the phase-separated system and which allows reagents from the continuous and discontinuous phases to react at the interface. Previous research in the Pentzer lab demonstrated that GO nanosheets and their modified derivatives are suitable surfactants: as-prepared GO can stabilize emulsions in which water is the continuous phase, whereas GO modified with primary alkyl amines (alkylated GO) can stabilize emulsions with a continuous phase of oil (e.g., octane).[53] In this work, we templated capsule formation using water-free emulsions stabilized by GO modified with octadecylamine (C_{18}−GO), thereby preventing undesired hydrolysis of isocyanates into primary amines.

Capsule Formation in DMF-in-Octane Emulsions Stabilized by C_{18}−GO. GO nanosheets were prepared by the oxidation of graphite flakes using potassium permanganate and sulfuric acid at room temperature, that is, a modified Hummer's method.[52−54] These nanosheets were dispersed in DMF and functionalized with octadecylamine at 55 °C to produce alkylated GO which could be isolated by centrifugation and redispersed in octane. FTIR spectroscopy confirmed the successful formation of GO and C_{18}−GO (Figure S3).

Oil-in-oil emulsions were formed by adding anhydrous DMF to an octane dispersion of C_{18}−GO (2.0 mg/mL) and then agitating using a hand-held tissue-tearor. Capsules were prepared by dissolving diisocyanate, TEG, and TEA in the dispersed phase (DMF), forming the emulsion, and then adding diamine and DBTDA to the continuous octane phase (mole ratio of diisocyanate and diamine controlled at approximately 3:1). TEG was used to form the polyurethane segment, which has been shown to optimize the tensile property of the polymer and gives a glass transition temperature that enables efficient bond exchange; TEA was used to form crosslinks in the polymer, and DBTDA was used as a catalyst to promote urethane bond formation. Notably, these reagents are used in the synthesis of bulk polymers containing HUBs. To evaluate the impact of steric hindrance of the diamine on the formation and dynamic properties of capsule shells, secondary diamines with different substituents were employed: *t*-butyl groups (DTEDA), *iso*-propyl groups (DIEDA), and ethyl groups (DEEDA). To evaluate if isocyanate identity impacts capsule formation and shell dynamicity, both aliphatic (HDI and CHDI) and aromatic (BZDI and mXDI) diisocyanates were used.

Temperature-Dependent Capsule Shell Bonding and Destruction. Figure 1Ai−iii shows successful capsule formation using the diisocyanate CHDI and the three different diamines (DTEDA, DIEDA, and DEEDA). Capsules were isolated by gravity filtration and then redispersed in dodecane and deposited on a glass slide, which showed individual capsules under an optical microscope. It is obvious that diamine identity can influence the capsule size and shell morphology: CHDI × DTEDA capsules range from 5 to 10 μm in diameter, CHDI × DIEDA capsules are 25−50 μm, and CHDI × DEEDA capsules are 5−20 μm (Table 1, first column). Further, the CHDI × DEEDA capsules are more irregular and less spherical compared to the other two. The differences in size and morphology can be attributed to the solubility of monomers and oligomers in the two phases, which likely impacts the location of interfacial polymerization.[15,55] FTIR spectroscopy (Figure 1B) and TGA weight loss profiles (Figure 1C) were employed to characterize the capsules. In Figure 1B, the peaks at approximately 3310 and 1525 cm^{-1} are attributed to the N−H stretching and bending of the urea and urethane linkages in the polymers, whereas the peaks at 1625 and 1695 cm^{-1} correspond to the C═O bond of urea and urethane, respectively. These characteristic peaks in the FTIR spectra indicate the successful fabrication of hindered poly(urea-urethane)s shells. The TGA weight loss profiles for all capsules show a majority of weight loss occurred from 180 to 500 °C, which is consistent with literature values for the bulk polymer.[46]

To determine the impact of the HUBs in the capsule shell, we sought to demonstrate the following: (1) formation of monoliths by bond exchange between neighboring capsule shells and (2) destruction of capsule shells by addition of

https://doi.org/10.1021/acs.chemmater.2c00415
Chem. Mater. 2022, 34, 5821−5831

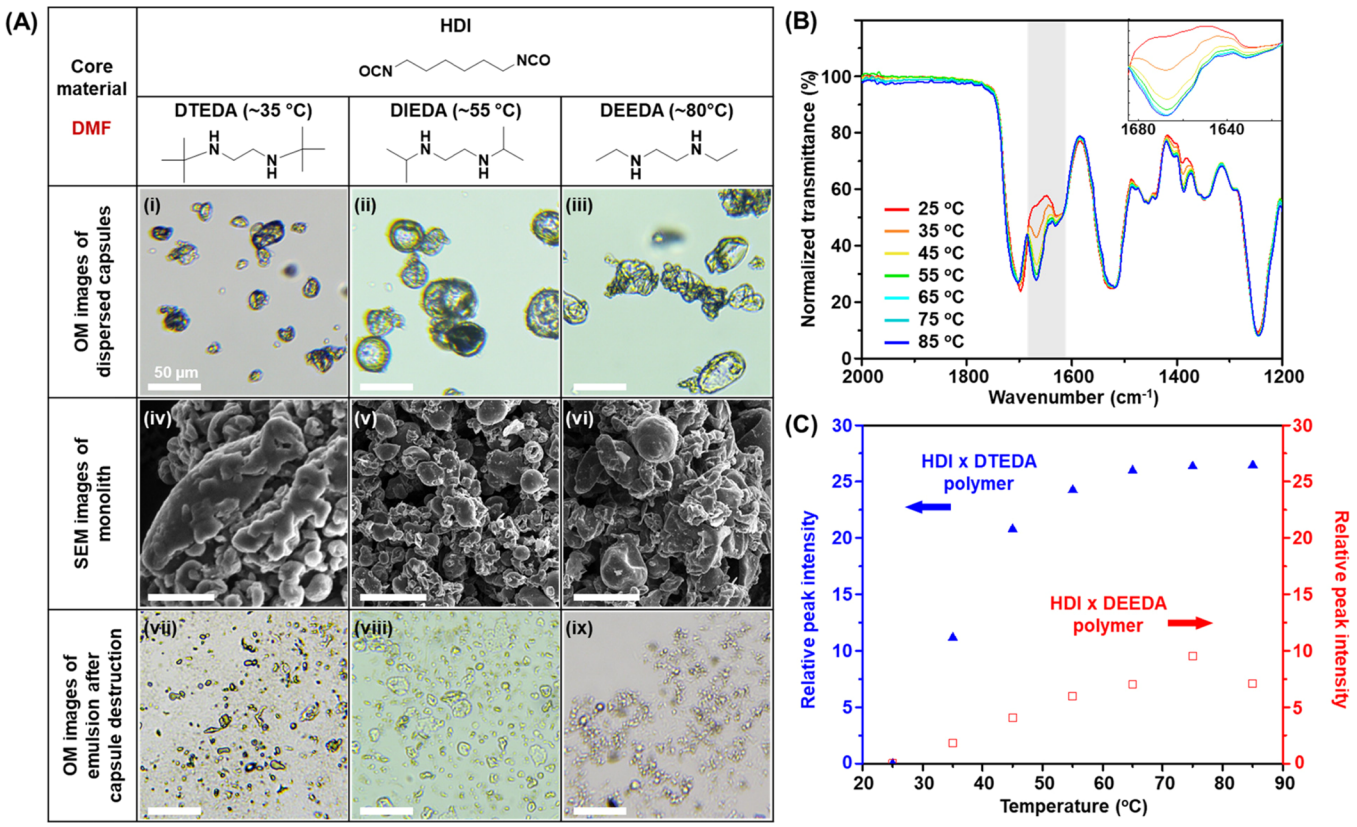

Figure 2. (A) HDI × DTEDA/DIEDA/DEEDA capsules with the DMF core: optical microscopy images of capsules redispersed in dodecane (i–iii), SEM images of monoliths (iv–vi), and optical microscopy images after capsule shell destruction (vii–ix), scale bars are 50 μm; (B) normalized VT-FTIR spectra of the HDI × DTEDA polymer at different temperatures, inset shows spectra from 1685 to 1615 cm^{-1}; and (C) relative intensity of peaks at ~1668 cm^{-1} for HDI × DTEDA and HDI × DEEDA polymer at different temperatures.

primary alkyl amines. The CHDI capsule family was chosen to demonstrate these changes. The identity of the diamine dictated the temperature at which the bonds could be efficiently exchanged: for capsules with DTEDA, DIEDA, and DEEDA, shell fusion or destruction occurred at approximately 35, 55, and 80 °C, respectively. This difference supports that the dynamic property of the capsule shell is controlled by the hindrance of the diamine, much like what is observed with the bulk polymer samples. The shells of dry capsules were chemically bonded to each other by heating after compaction via solvent evaporation or being put in a mold. Figure 1Aiv–vi shows SEM images of samples isolated after capsule fusion, where monoliths are observed and there are no individual capsules, though the texture of the monoliths may be attributed to the initial capsule structure. In contrast, Figure 1Avii–ix shows optical microscopy images after addition of primary amines and capsule shell destruction. These are markedly different from the appearance of redispersed capsules, whereas the capsule surfaces are textured and have wrinkles, and after destruction, the droplets have a smooth surface. Unlike the emulsions stabilized only by C_{18}–GO, the emulsion droplets produced after shell destruction have different shapes (spherical, elliptical, peanut, irregular, etc.), which may be attributed to the multiple surfactants that are present (C_{18}–GO and PUU oligomers). These results demonstrate that the HUBs in the capsule shell enable bond exchange for capsule shell fusion and destruction dependent on the reaction conditions. Additionally, the responsive temperatures of efficient bond exchange are quite similar to those in the homogeneous (bulk) systems, which indicates that the nonpolar/nonionic solvent does not significantly impact the dynamicity of the polymer shell.

Figure 2A highlights shell fusion and destruction of capsules prepared with HDI as the diisocyanate and the same three diamines. FTIR and TGA characterization data of these capsules can be found in Figures S4 and S5 and are consistent with the formation of the expected HPUU. As shown in Figure 2Ai–iii, HDI × DTEDA capsules have diameters ranging from 5 to 25 μm, while HDI × DIEDA capsules have diameters 25–50 μm, and the majority of HDI × DEEDA capsules are 20–40 μm in diameter (Table 1, second column). The difference of size distribution among capsules prepared using the same diamine but different diisocyanates illustrates that the isocyanate identity can also influence the size of the capsules formed, with alkyl diisocyanate giving larger capsules in most cases (Table 1). Comparison of optical microscopy images of capsules without post-processing (continuous phase removal and redispersion in dodecane, Figure S6) and with post-processing (isolated and redispersed Figure 2Ai–iii), supports that post-processing can impact the sphericity and aggregation of the capsules, likely due to collapse upon removal of the core liquid. FIB-SEM images confirm that the capsules have a core-shell structure and reveal that the shell thickness ranges from ~1.5 to a few microns (Figure S7); notably, some capsules may have crosslinks inside, which can be attributed to the diffusion of diamines into the DMF. For HDI × DTEDA/DIEDA/DEEDA capsules, shell fusion and destruction were achieved at 35, 55, and 80 °C (Figure 2Aiv–ix), again corresponding to

https://doi.org/10.1021/acs.chemmater.2c00415
Chem. Mater. 2022, 34, 5821–5831

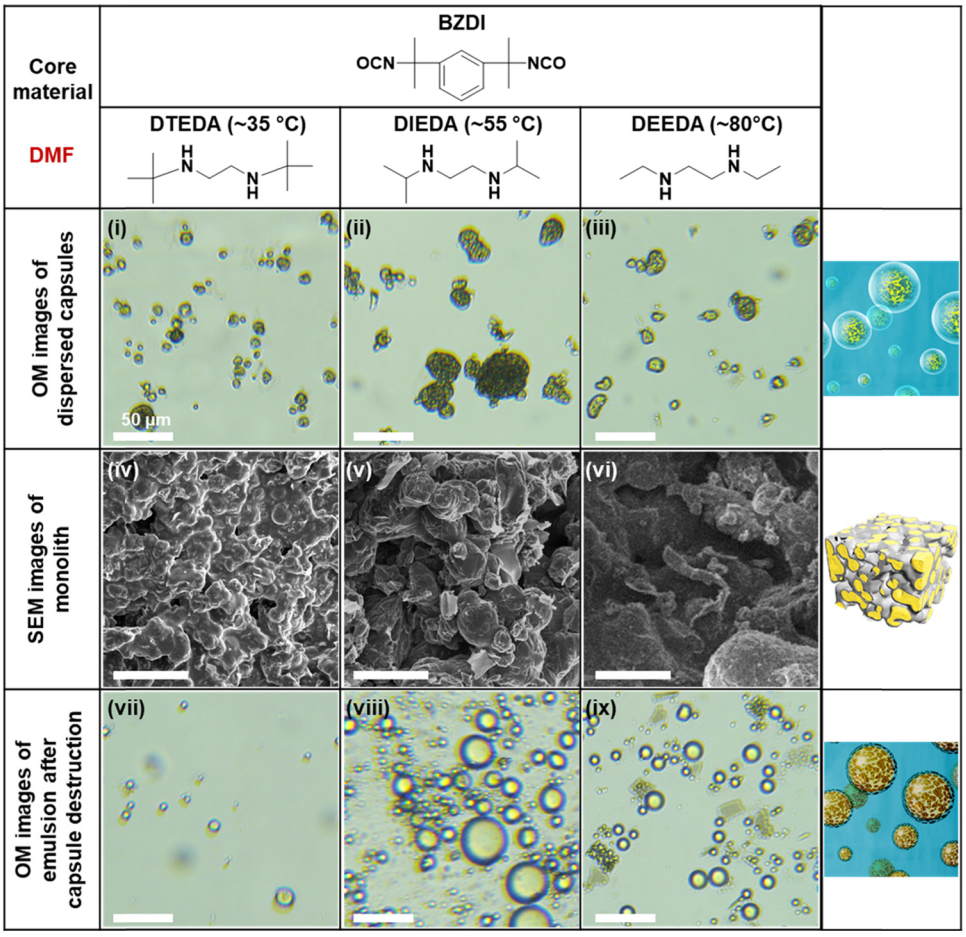

Figure 3. Optical microscopy images of individual capsules redispersed in dodecane (i–iii), SEM images of monoliths (iv–vi), and optical microscopy images after capsule destruction (vii–ix) for BZDI × DTEDA/DIEDA/DEEDA capsules with a core of DMF. Scale bars are 50 μm.

the different hindered diamine used. The temperature required is similar to that for the CHDI × DTEDA/DIEDA/DEEDA capsules, indicating that these two isocyanates have limited impact on the temperature required for bond exchange and the dynamicity is mainly controlled by the hindered amine.

In addition to CHDI and HDI, the diisocyanate mXDI was also employed with the same three secondary diamines to prepare capsules with HUBs in the shells (Figure S8 and Table 1, fourth column). Briefly, similar responsive properties and diamine-dependent temperature requirements were observed for these capsules as for the CHDI and HDI capsule families. These results support that the hindrance of amine is the main factor that impacts the responsive temperature of the HUBs in capsule shells.

VT-FTIR Studies of HUB Reversibility. To further confirm that the dynamic property of the capsule shell comes from the HPUU chemistry, and the hindrance of diamine determines the dynamicity, variable-temperature FTIR spectroscopy was used to evaluate changes in the carbonyl region during heating (Figures S9 and S10). Figure 2B shows the normalized FTIR spectra of polymers containing HDI × DTEDA at temperatures from 25 to 85 °C (the temperature for capsule fusion or destruction is 35 °C). Upon increasing the temperature, a peak at 1668 cm^{-1} becomes apparent, which we attribute to a carbonyl-containing intermediate formed during the bond exchange process (the peak disappears as the sample is cooled). Figure S11 shows the FTIR spectra over the same temperature range for the HDI × DEEDA polymer (the temperature for capsule fusion or destruction is 80 °C), revealing a similar trend. To better represent this data, Figure 2C compares the relative peak intensity for both polymer systems as a function of temperature. The HDI × DTEDA polymer displays an increase in the intensity of the peak at 1668 cm^{-1} by 11.2% upon heating from 25 to 35 °C; in contrast, the HDI × DEEDA polymer requires heating to at least 75 °C to achieve approximately the same peak intensity increase (9.5%). This difference supports that hindrance of the diamine controls the responsivity of HUBs.

Capsules with IL in the Core. Our group has shown that encapsulation of viscous liquids, such as ILs, facilitates their transport, storage, and application in, for example, energy storage and gas uptake. As such, we sought to expand the encapsulation system demonstrated above to include capsules with IL cores. Initial attempts to use pure IL as the discontinuous phase did not lead to the formation of capsules stable at room temperature (i.e., capsule shells would fuse); we attribute this to a plasticization of the polymer shell with the IL, which provides a more polar environment; this may effectively stabilize an intermediate and decrease the activation energy required for the dynamic bond exchange. With this information in hand, we then used mixtures of DMF and IL (3:1 ratio) as the discontinuous phase in the emulsions (i.e., droplets), which we found to give stable individual capsules when cooled to ~2 °C.

https://doi.org/10.1021/acs.chemmater.2c00415
Chem. Mater. 2022, 34, 5821–5831

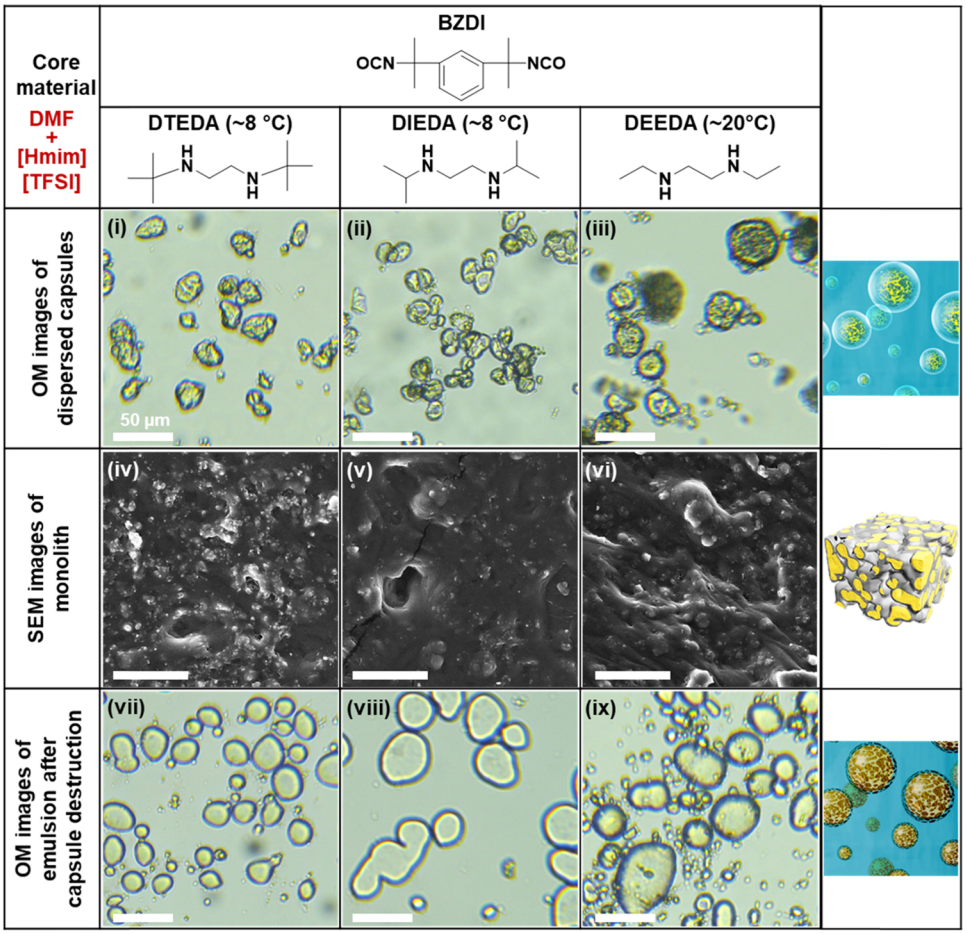

Figure 4. Optical microscopy images of individual capsules redispersed in dodecane (i–iii), SEM images of monoliths (iv–vi), and optical microscopy images after capsule destruction (vii–ix) for BZDI × DTEDA/DIEDA/DEEDA capsules with a core of DMF/[Hmim][TFSI]. Scale bars are 50 μm.

Figures 3 and 4 show individual BZDI × DTEDA/DIEDA/DEEDA capsules and their dynamic behavior with and without the presence of [Hmim][TFSI] in the core. In the absence of IL, BZDI × DTEDA capsule diameters are generally ≤10 μm, BZDI × DIEDA capsules are between 10 and 50 μm, and BZDI × DEEDA capsules are 10–20 μm. For capsules with IL/DMF cores, BZDI × DTEDA capsules are larger (20–25 μm), BZDI × DIEDA capsules are similar (15–20 μm), and BZDI × DEEDA capsules are larger (25–40 μm), as summarized in the third column of Table 1. This indicates that not only the monomer identity but also the encapsulated liquid influences the size of capsules, with the IL-containing capsules generally being larger and having a narrower size distribution. The FTIR spectra for BZDI × DTEDA/DIEDA/DEEDA capsules without IL (Figure S12) are similar to those of the CHDI/HDI/mXDI × DTEDA/DIEDA/DEEDA capsules described above. For the IL-containing capsules, FTIR stretching frequencies at 1348, 1180, and 1136 cm^{-1} indicate the presence of the IL (Figures S13 and S14). In TGA weight loss profiles, all capsules show a significant weight loss from 180 to 500 °C, but the IL-containing capsules have an additional weight loss from 300 to 450 °C (~33 wt%, Figure 5). As this higher temperature weight loss is consistent with neat IL (Figure S15), these data support the successful encapsulation of [Hmim][TFSI] as a mixture with DMF.

To measure the wt% of encapsulated IL, the core liquid was extracted using acetone-d^6 containing mesitylene as an internal standard, along with ^{1}H NMR spectroscopy (Figure S2). The peak at 2.09 ppm corresponds to the proton of the methyl groups of mesitylene, and the peak at 3.65 ppm corresponds to the protons of the methyl group on the nitrogen of the imidazolium. Thus, the ratio of the integral of the peak at 2.09 ppm to that of the peak at 3.65 ppm can be used to calculate the wt% of IL encapsulated (Table S2). Table S3 shows that the average calculated IL wt% for BZDI × DTEDA/DIEDA/DEEDA capsules are 33.5, 35.0, and 36.2 wt%, respectively, which are close to the 33 wt% supported by TGA data, further proving the successful encapsulation (each sample was measured 3 times and averaged).

The identity of the core materials also dictates the temperature-responsive features of the HUB-containing capsule shells. With capsules in which DMF is the core, the monoliths formed retained artifacts of the initial capsule structures, as observed by SEM (Figure 3iv–vi). However, when capsules with hybrid cores of DMF/IL are treated under the same conditions, the monoliths are smoother and do not have identifiable structures that could be attributed to capsules (Figure 4iv–vi). Another interesting phenomenon observed is that the temperature for capsule shell bonding and destruction of the IL-containing capsule is much lower than that of the same shell with only DMF in the core (~8 °C for BZDI × DTEDA/DIEDA capsules and ~20 °C for the BZDI × DEEDA capsule). Again, this difference may be because the polarity of the IL can better stabilize charged intermediates

https://doi.org/10.1021/acs.chemmater.2c00415
Chem. Mater. 2022, 34, 5821–5831

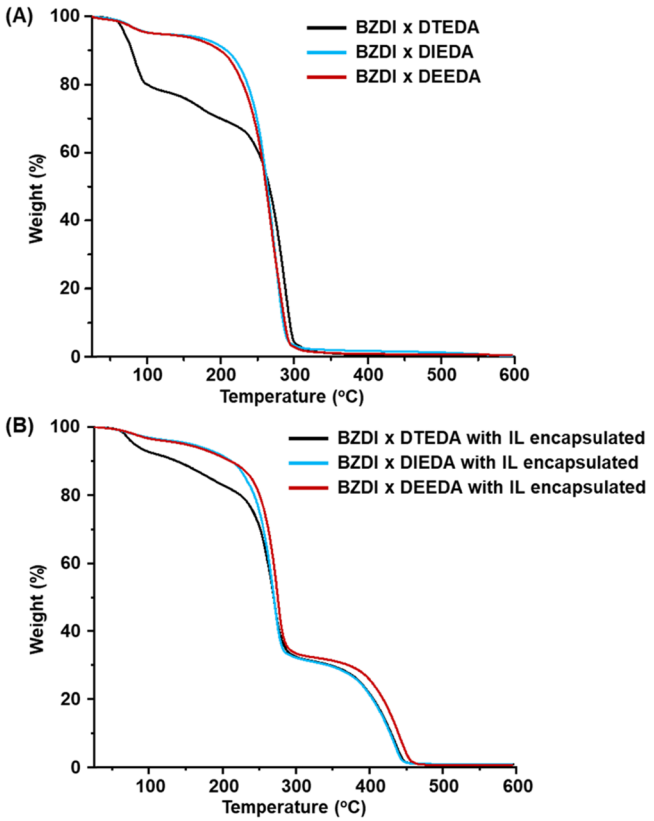

Figure 5. TGA weight loss profiles of BZDI × DTEDA/DIEDA/DEEDA capsules without (A) and with (B) [Hmim][TFSI] in the core.

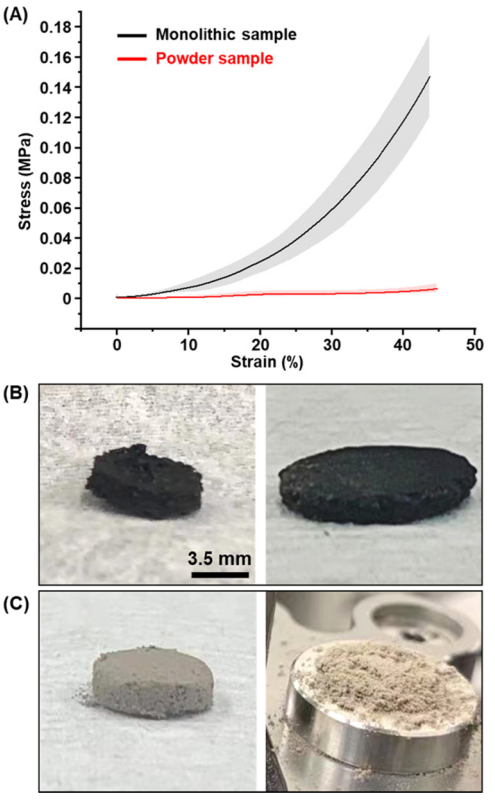

Figure 6. (A) DMA compression test results for mXDI × DTEDA capsule powder (red) and monolith (black), shaded area is error bar; (B) photographs of the monolithic sample before (left) and after (right) compression; and (C) photographs of the powder sample before (left) and after (right) compression.

formed during bond exchange, guiding future polymer design considerations.

Impact of Capsule Fusion. Whereas capsules can benefit the transport and handling of liquids, access to monolith samples can be desired for specific applications or operating conditions. To characterize the macroscopic properties of the monolith formed upon capsule shell fusion, DMA compression tests of cylinders were carried out for the capsule powder and their corresponding monoliths produced upon dynamic bond exchange for the mXDI × DTEDA system. To test the powders, cylinders of capsule powder were placed onto the test stage. To test the monoliths, cylinders were formed by putting the capsule powder into a cylindrical mold and heating overnight at 35 °C and then placing it onto the test stage. The darker color of the monolith sample (Figure 6B) compared to that of the powder sample (Figure 6C) can be attributed to slight thermal reduction of the nanosheets during the heating process. Figure 6A shows stress−strain curves of the two samples, where the nearly flat red curve is consistent with the collapsed powder shown in Figure 6C, and the black curve shows that the monolith can resist compression (0.146 MPa to 45% specimen length change, Figure 6A,B). These data confirm the successful capsule bonding from the macroscopic perspective and demonstrate the impact on bulk properties.

CONCLUSIONS

In this study, we prepare, for the first time, capsules bearing dynamic covalent bonds in the polymer shell, with a liquid core. Shells based on HPUU chemistry were successfully fabricated, with capsule size and morphology impacted by the identity of the monomers and core liquid. Mild heating can be used to fuse the capsules into monolithic materials or destroy the capsule shell in the presence of a primary amine, changes that were confirmed by optical microscopy, SEM, and compression test. For capsules with a core of DMF, the temperature for bond exchange is controlled by the identity of the diamine, as with the bulk polymer, which was confirmed by variable-temperature FTIR spectroscopy. In contrast, capsules with core mixtures of DMF and IL required significantly lower temperature for bond exchange, suggesting that the capsule shell is plasticized with the core material, and indicating a route forward to controlling responsive properties. The results presented herein provide a template for preparing thermo-responsive dynamic capsules which can be generalized to different emulsion components (continuous phase and dispersed phase), surfactants, and chemical reagents, as well as the production of other structures (e.g., hollow capsules), which have broad relevance to energy storage, molecular separation, gas storage, biomedicine, and so on. This system is in direct contrast to most responsive capsules which undergo changes in shell permeability based on pH or temperature and opens possibilities, for example, for integration of liquids into monolithic structures in a single synthetic step.

ASSOCIATED CONTENT

Supporting Information

The Supporting Information is available free of charge at https://pubs.acs.org/doi/10.1021/acs.chemmater.2c00415.

https://doi.org/10.1021/acs.chemmater.2c00415
Chem. Mater. 2022, 34, 5821−5831

Additional FTIR, TGA, optical microscopy, and SEM characterization of capsules and IL; ^{1}H NMR spectrum of extraction of [Hmim][TFSI]; variable-temperature FTIR setup and spectra analysis; FIB-SEM of selected capsules; list of reagents for producing capsules; calculation methodology; and calculated IL wt% of IL-containing capsules (PDF)

AUTHOR INFORMATION

Corresponding Author

Emily Pentzer − *Department of Materials Science & Engineering and Department of Chemistry, Texas A&M University, College Station, Texas 77843, United States;* orcid.org/0000-0001-6187-6135; Email: emilypentzer@tamu.edu

Authors

Yifei Wang − *Department of Materials Science & Engineering, Texas A&M University, College Station, Texas 77843, United States;* orcid.org/0000-0003-0110-8147

Peiran Wei − *Soft Matter Facility, Texas A&M University, College Station, Texas 77845, United States*

Qing Zhou − *Department of Materials Science & Engineering, Texas A&M University, College Station, Texas 77843, United States;* orcid.org/0000-0002-0908-5093

Ciera Cipriani − *Department of Materials Science & Engineering, Texas A&M University, College Station, Texas 77843, United States;* orcid.org/0000-0003-0473-8005

Miao Qi − *Department of Materials Science & Engineering, Texas A&M University, College Station, Texas 77843, United States*

Svetlana Sukhishvili − *Department of Materials Science & Engineering, Texas A&M University, College Station, Texas 77843, United States;* orcid.org/0000-0002-2328-4494

Complete contact information is available at: https://pubs.acs.org/10.1021/acs.chemmater.2c00415

Author Contributions

E.P. and Y.W. designed the project and majority of the experiments. Y.W. carried out all experiments and performed all characterizations except the compression test. P.W. designed the compression test and helped with preparing the samples and C.C. performed the test. P.W. designed and set up the VT-FTIR device and gave guidance for the test. Q.Z. processed the VT-FTIR data. S.S. helped to conceptualize the VT-FTIR experiments and interpret the data. M.Q. helped with the synthesis of bulk polymers. Y.W. wrote the first draft of the manuscript. All authors discussed the results and provided constructive comments on the final manuscript. All authors have given approval to the final version of the manuscript.

Notes

The authors declare no competing financial interest.

ACKNOWLEDGMENTS

The authors thank NSF DMR Award #2103182 and Texas A&M University for financial support. The authors acknowledge the use of the Soft Matter Facility and Microscopy and Imaging Center Core Facility at Texas A&M. The authors thank Dr. Sisi Xiang at Materials Characterization Facility and Mr. Jung Hwan Woo at AggieFab Nanofabrication Facility of Texas A&M for FIB-SEM.

REFERENCES

(1) Zhang, Q.; Chen, Y.; Lu, R.; Yao, Y.; Li, C.; Yu, Y.; Zhang, S. Cross-linked small-molecule capsules with excitation wavelength-dependent photoluminescence and high loading capacity: design, synthesis and application in imaging-guided drug delivery. *J. Mater. Chem. B* **2020**, *8*, 2719−2725.

(2) Ping, Y.; Guo, J.; Ejima, H.; Chen, X.; Richardson, J. J.; Sun, H.; Caruso, F. pH-Responsive Capsules Engineered from Metal-Phenolic Networks for Anticancer Drug Delivery. *Small* **2015**, *11*, 2032−2036.

(3) Cui, L.; Wang, R.; Ji, X.; Hu, M.; Wang, B.; Liu, J. Template-assisted synthesis of biodegradable and pH-responsive polymer capsules via RAFT polymerization for controlled drug release. *Mater. Chem. Phys.* **2014**, *148*, 87−95.

(4) Shi, D.; Ran, M.; Huang, H.; Zhang, L.; Li, X.; Chen, M.; Akashi, M. Preparation of glucose responsive polyelectrolyte capsules with shell crosslinking via the layer-by-layer technique and sustained release of insulin. *Polym. Chem.* **2016**, *7*, 6779−6788.

(5) Marturano, V.; Bizzarro, V.; De Luise, A.; Calarco, A.; Ambrogi, V.; Giamberini, M.; Tylkowski, B.; Cerruti, P. Essential oils as solvents and core materials for the preparation of photo-responsive polymer nanocapsules. *Nano Res.* **2018**, *11*, 2783−2795.

(6) Zhao, Y.; Lv, L.-P.; Jiang, S.; Landfester, K.; Crespy, D. Advanced stimuli-responsive polymer nanocapsules with enhanced capabilities for payloads delivery. *Polym. Chem.* **2015**, *6*, 4197−4205.

(7) Liu, H.; Wang, X.; Wu, D.; Ji, S. Fabrication and applications of dual-responsive microencapsulated phase change material with enhanced solar energy-storage and solar photocatalytic effectiveness. *Sol. Energy Mater. Sol. Cells* **2019**, *193*, 184−197.

(8) Kitayama, Y.; Takeuchi, T. Photodegradable Polymer Capsules Fabricated via Interfacial Photocross-linking of Spherical Polymer Particles. *ACS Appl. Polym. Mater.* **2020**, *2*, 3813−3820.

(9) Kitayama, Y.; Harada, A. Interfacial Photo-Cross-Linking: Simple but Powerful Approach for Fabricating Capsule Polymer Particles with Tunable pH-Responsive Controlled Release Capability. *ACS Appl. Mater. Interfaces* **2021**, *13*, 10359−10375.

(10) Zeng, Z.; Wen, M.; Ye, G.; Huo, X.; Wu, F.; Wang, Z.; Yan, J.; Matyjaszewski, K.; Lu, Y.; Chen, J. Controlled Architecture of Hybrid Polymer Nanocapsules with Tunable Morphologies by Manipulating Surface-Initiated ARGET ATRP from Hydrothermally Modified Polydopamine. *Chem. Mater.* **2017**, *29*, 10212−10219.

(11) Yao, Y.; Yu, Y.; Wan, X.; Yan, D.; Chen, Y.; Luo, J.; Vancso, G. J.; Zhang, S. Azobenzene-Based Cross-Linked Small-Molecule Vesicles for Precise Oxidative Damage Treatments Featuring Controlled and Prompt Molecular Release. *Chem. Mater.* **2021**, *33*, 7357−7366.

(12) Huang, X.; Appelhans, D.; Formanek, P.; Simon, F.; Voit, B. Synthesis of Well-Defined Photo-Cross-Linked Polymeric Nanocapsules by Surface-Initiated RAFT Polymerization. *Macromolecules* **2011**, *44*, 8351−8360.

(13) Huang, X.; Appelhans, D.; Formanek, P.; Simon, F.; Voit, B. Tailored synthesis of intelligent polymer nanocapsules: an investigation of controlled permeability and pH-dependent degradability. *ACS Nano* **2012**, *6*, 9718−9726.

(14) Menard, M.; Meyer, F.; Parkhomenko, K.; Leuvrey, C.; Francius, G.; Begin-Colin, S.; Mertz, D. Mesoporous silica templated-albumin nanoparticles with high doxorubicin payload for drug delivery assessed with a 3-D tumor cell model. *Biochim. Biophys. Acta, Gen. Subj.* **2019**, *1863*, 332−341.

(15) Luo, Q.; Wang, Y.; Chen, Z.; Wei, P.; Yoo, E.; Pentzer, E. Pickering emulsion-templated encapsulation of ionic liquids for contaminant removal. *ACS Appl. Mater. Interfaces* **2019**, *11*, 9612−9620.

(16) Natour, S.; Levi-Zada, A.; Abu-Reziq, R. Magnetic Polyurea Nano-Capsules Synthesized via Interfacial Polymerization in Inverse Nano-Emulsion. *Molecules* **2019**, *24*, 2663.

(17) Vazquez-Mera, N. A.; Otaegui, J. R.; Sanchez, R. S.; Prats, G.; Guirado, G.; Ruiz-Molina, D.; Roscini, C.; Hernando, J. Color-Tunable White-Light-Emitting Materials Based on Liquid-Filled

Capsules and Thermally Responsive Dyes. *ACS Appl. Mater. Interfaces* **2019**, *11*, 17751−17758.
(18) Xu, S.; Nisisako, T. Polymer Capsules with Tunable Shell Thickness Synthesized via Janus-to-core shell Transition of Biphasic Droplets Produced in a Microfluidic Flow-Focusing Device. *Sci. Rep.* **2020**, *10*, 4549.
(19) Yi, H.; Yang, Y.; Gu, X.; Huang, J.; Wang, C. Multilayer composite microcapsules synthesized by Pickering emulsion templates and their application in self-healing coating. *J. Mater. Chem. A* **2015**, *3*, 13749−13757.
(20) Weiss, E.; Dutta, B.; Kirschning, A.; Abu-Reziq, R. BMIm-PF_6@SiO_2 Microcapsules: Particulated Ionic Liquid as A New Material for the Heterogenization of Catalysts. *Chem. Mater.* **2014**, *26*, 4781−4787.
(21) Uebel, F.; Thérien-Aubin, H.; Landfester, K. Glycerol-based polyurethane nanoparticles reduce friction and wear of lubricant formulations. *Macromol. Mater. Eng.* **2021**, *307*, No. 2100821.
(22) Edgehouse, K. J.; Rosenfeld, N.; Bergbreiter, D. E.; Pentzer, E. B. Capsules of the Poly(α-olefin) PAO432 for Removal of BTEX Contaminants from Water. *Ind. Eng. Chem. Res.* **2021**, *60*, 14455−14463.
(23) Wang, Y.; Quevedo, K.; Pentzer, E. Inter-capsule fusion and capsule shell destruction using dynamic covalent polymers. *Polym. Chem.* **2021**, *12*, 2695−2700.
(24) Luo, Q.; Pentzer, E. Encapsulation of Ionic Liquids for Tailored Applications. *ACS Appl. Mater. Interfaces* **2020**, *12*, 5169−5176.
(25) Huang, Q.; Luo, Q.; Wang, Y.; Pentzer, E.; Gurkan, B. Hybrid Ionic Liquid Capsules for Rapid CO_2 Capture. *Ind. Eng. Chem. Res.* **2019**, *58*, 10503−10509.
(26) Chakma, P.; Konkolewicz, D. Dynamic Covalent Bonds in Polymeric Materials. *Angew. Chem., Int. Ed. Engl.* **2019**, *58*, 9682−9695.
(27) Zheng, N.; Xu, Y.; Zhao, Q.; Xie, T. Dynamic Covalent Polymer Networks: A Molecular Platform for Designing Functions beyond Chemical Recycling and Self-Healing. *Chem. Rev.* **2021**, *121*, 1716−1745.
(28) Accardo, J. V.; McClure, E. R.; Mosquera, M. A.; Kalow, J. A. Using Visible Light to Tune Boronic Acid-Ester Equilibria. *J. Am. Chem. Soc.* **2020**, *142*, 19969−19979.
(29) Cash, J. J.; Kubo, T.; Bapat, A. P.; Sumerlin, B. S. Room-Temperature Self-Healing Polymers Based on Dynamic-Covalent Boronic Esters. *Macromolecules* **2015**, *48*, 2098−2106.
(30) Lei, Z. Q.; Xiang, H. P.; Yuan, Y. J.; Rong, M. Z.; Zhang, M. Q. Room-temperature self-healable and remoldable cross-linked polymer based on the dynamic exchange of disulfide bonds. *Chem. Mater.* **2014**, *26*, 2038−2046.
(31) Otsuka, H.; Nagano, S.; Kobashi, Y.; Maeda, T.; Takahara, A. A dynamic covalent polymer driven by disulfide metathesis under photoirradiation. *Chem. Commun.* **2010**, *46*, 1150−1152.
(32) Kovaricek, P.; Lehn, J.-M. Merging constitutional and motional covalent dynamics in reversible imine formation and exchange processes. *J. Am. Chem. Soc.* **2012**, *134*, 9446−9455.
(33) Boutelle, R. C.; Northrop, B. H. Substituent effects on the reversibility of furan−maleimide cycloadditions. *J. Org. Chem.* **2011**, *76*, 7994−8002.
(34) Ehrhardt, D.; Mangialetto, J.; Van Durme, K.; Van Mele, B.; Van den Brande, N. From Slow to Fast Self-Healing at Ambient Temperature of High-Modulus Reversible Poly (methacrylate) Networks. Single-and Dual-Dynamics and the Effect of Phase Separation. *Macromolecules* **2021**, *54*, 9960−9977.
(35) Lu, Y.-X.; Guan, Z. Olefin metathesis for effective polymer healing via dynamic exchange of strong carbon−carbon double bonds. *J. Am. Chem. Soc.* **2012**, *134*, 14226−14231.
(36) Huang, S.; Kong, X.; Xiong, Y.; Zhang, X.; Chen, H.; Jiang, W.; Niu, Y.; Xu, W.; Ren, C. An overview of dynamic covalent bonds in polymer material and their applications. *Eur. Polym. J.* **2020**, *141*, No. 110094.
(37) Accardo, J. V.; Kalow, J. A. Reversibly tuning hydrogel stiffness through photocontrolled dynamic covalent crosslinks. *Chem. Sci.* **2018**, *9*, 5987−5993.
(38) Zhang, B.; Ke, J.; Vakil, J. R.; Cummings, S. C.; Digby, Z. A.; Sparks, J. L.; Ye, Z.; Zanjani, M. B.; Konkolewicz, D. Dual-dynamic interpenetrated networks tuned through macromolecular architecture. *Polym. Chem.* **2019**, *10*, 6290−6304.
(39) Zhou, Q.; Gardea, F.; Sang, Z.; Lee, S.; Pharr, M.; Sukhishvili, S. A. A Tailorable Family of Elastomeric-to-Rigid, 3D Printable, Interbonding Polymer Networks. *Adv. Funct. Mater.* **2020**, *30*, No. 2002374.
(40) Zhang, Q.; Wang, S.; Rao, B.; Chen, X.; Ma, L.; Cui, C.; Zhong, Q.; Li, Z.; Cheng, Y.; Zhang, Y. Hindered urea bonds for dynamic polymers: An overview. *React. Funct. Polym.* **2021**, *159*, No. 104807.
(41) Sun, W.; Luo, J.; Zhang, L.; Chen, Y.; Li, P.; Zheng, Y.; Cheng, Y. Insulating Silicones Based on Dynamic Hindered Urea Bonds with High Dielectric Healability and Recyclability. *ACS Appl. Polym. Mater.* **2021**, *3*, 5622−5631.
(42) Chen, M.; Feng, X.; Xu, W.; Wang, Y.; Yang, Y.; Jiang, Z.; Ding, J. PEGylated Polyurea Bearing Hindered Urea Bond for Drug Delivery. *Molecules* **2019**, *24*, 1538.
(43) Ying, H.; Cheng, J. Hydrolyzable polyureas bearing hindered urea bonds. *J. Am. Chem. Soc.* **2014**, *136*, 16974−16977.
(44) Ying, H.; Zhang, Y.; Cheng, J. Dynamic urea bond for the design of reversible and self-healing polymers. *Nat. Commun.* **2014**, *5*, 3218.
(45) Zhang, L.; Rowan, S. J. Effect of Sterics and Degree of Cross-Linking on the Mechanical Properties of Dynamic Poly(alkylurea−urethane) Networks. *Macromolecules* **2017**, *50*, 5051−5060.
(46) Ying, H. *Hindered urea bond for the design of dynamic materials*. PhD thesis, University of Illinois at Urbana-Champaign, 2017.
(47) Erice, A.; de Luzuriaga, A. R.; Matxain, J. M.; Ruipérez, F.; Asua, J. M.; Grande, H.-J.; Rekondo, A. Reprocessable and recyclable crosslinked poly (urea-urethane) s based on dynamic amine/urea exchange. *Polymer* **2018**, *145*, 127−136.
(48) Sun, W.; Zhang, L.; Wang, S.; Mao, J.; Luo, J.; Chen, Y.; Cheng, Y. Mechanically enhanced healable and recyclable silicone with dynamic hindered urea bond for flexible electronics. *J. Mater. Chem. C* **2021**, *9*, 8579−8588.
(49) Luo, Q.; Wei, P.; Huang, Q.; Gurkan, B.; Pentzer, E. B. Carbon capsules of ionic liquid for enhanced performance of electrochemical double-layer capacitors. *ACS Appl. Mater. Interfaces* **2018**, *10*, 16707−16714.
(50) Wei, P.; Cipriani, C. E.; Pentzer, E. B. Thermal energy regulation with 3D printed polymer-phase change material composites. *Matter* **2021**, *4*, 1975−1989.
(51) Cipriani, C. E.; Ha, T.; Martinez Defilló, O. B.; Myneni, M.; Wang, Y.; Benjamin, C. C.; Wang, J.; Pentzer, E. B.; Wei, P. Structure−processing−property relationships of 3D printed porous polymeric materials. *ACS Mater. Au* **2021**, *1*, 69−80.
(52) Dimiev, A.; Kosynkin, D. V.; Alemany, L. B.; Chaguine, P.; Tour, J. M. Pristine graphite oxide. *J. Am. Chem. Soc.* **2012**, *134*, 2815−2822.
(53) Rodier, B.; de Leon, A.; Hemmingsen, C.; Pentzer, E. Controlling oil-in-oil pickering-type emulsions using 2D materials as surfactant. *ACS Macro Lett.* **2017**, *6*, 1201−1206.
(54) Luo, Q.; Wang, Y.; Yoo, E.; Wei, P.; Pentzer, E. Ionic liquid-containing pickering emulsions stabilized by graphene oxide-based surfactants. *Langmuir* **2018**, *34*, 10114−10122.
(55) Zou, S.; Hu, Y.; Wang, C. One-Pot Fabrication of Rattle-Like Capsules with Multicores by Pickering-Based Polymerization with Nanoparticle Nucleation. *Macromol. Rapid Commun.* **2014**, *35*, 1414−1418.

https://doi.org/10.1021/acs.chemmater.2c00415
Chem. Mater. 2022, 34, 5821−5831